Rev. Roum. Sci. Techn.– Électrotechn. et Énerg.
Vol. **68**, *2*, pp. 121–126, Bucarest, 2023

NEW MODELING AND ENHANCED CONTROL STRATEGY FOR GRID-CONNECTED FOUR-LEG INVERTER WITHOUT PHASE-LOCKED LOOP AND PARK'S TRANSFORMATION

ALI CHEBABHI[1], ALA ADDIN MOHAMMED AL-DWA[1], MABROUK DEFDAF[1], ABDELHALIM KESSAL[2]

Keywords: Grid-connected four-leg inverter (GC-FLVSI); Enhanced voltage-oriented control (EVOC); Power control theory (DPC); Super twisting sliding mode control (STSMC); Static and dynamic performances.

This paper proposes an enhanced voltage-oriented control strategy (EVOC) based on super twisting sliding mode control (STSMC) for a grid-connected four-leg source voltage inverter (GC-FLVSI) in the synchronous rotating frame (dq0–frame) without using a phase-locked loop (PLL) and Park's transformation. The proposed strategy is used not only to control the dq0–axes FLVSI inject currents but also to derive the mathematical model of the GC-FLVSI in the dq0–frame based on the direct instantaneous power control theory (DPC) and to eliminate the impact of PLL and Park's transformation. The principle of the proposed EVOC strategy is analyzed in detail. The STSMC is used for accurate dq0–axes FLVSI inject current control, and it can result in sinusoidal currents with high quality, high robustness against parametric variations, and low chattering with easy implementation. Finally, the superiority of the proposed EVOC-STSMC strategy in terms of complexity, response, steady-state errors, robustness, total harmonic distortion (THDs) mitigation, neutral current reduction, and robustness against parameter variations is verified through comparative analysis with the EVOC strategy based on the PI controller (EVOC-PIC).

1. INTRODUCTION

During recent years, grid-connected four-leg source voltage inverters (GC-FLVSI) in distributed generation sources based on renewable energy sources (RER), including solar and wind energy technologies, have been proposed for transforming, controlling, and delivering the maximal power from these RER systems into the grid, which is mandatory to overcome the challenges of the traditional grid-connected three leg VSI, such as unbalanced grid voltages and currents under all conditions, including unbalanced single and three phase linear and nonlinear loads, and unbalanced grid voltages [1–3]. For the sake of achieving the desired functionality and performance, researchers in recent years have focused their research on the development of the appropriate control strategy for GC-FLVSI to achieve excellent static and dynamic performances, including decoupling effects, synchronization, simplicity, fast responses, zero steady-state errors, low injected current harmonic distortions, high robustness toward parametric variations and external disturbances, and high-efficiency.

The traditional vector-oriented control (VOC) strategy based on PLL in the dq0–frame is one of the most common control strategies available in the literature for these targets, which provides a time-invariant GC-FLVSI model in the dq0–frame [4–6]. Furthermore, ideal grid voltage conditions can provide predefined static and dynamic performance. However, in the presence of grid voltage disturbances such as voltage unbalance, voltage sag, and voltage harmonic distortions, the control performance of this strategy may deteriorate significantly, decreasing the static and dynamic performance of the GC-VSI systems [7, 8]. Moreover, the inherently complex PLL and the several Parks transformations used in these strategies increase the complexity of implementing the overall system [9].

To eliminate the impact of PLL and Park's transformation in the VOC strategy and to provide accurate current control with lower computational complexity, several enhancing VOC strategies without PLL and Park's transformation are proposed for GC-VSIs, such as VOC strategy based on coordinate transformation [10], VOC strategy based on direct power control (DPC) [11], VOC strategy based on grid voltage-modulated (GVM-VOC) [12], and VOC strategy based on nonlinear observed grid-phase [13]. These VOC strategies have many advantages and disadvantages linked to the static and dynamic performances and simplicity of implementation.

The VOC strategy based on DPC concepts can provide a linear time-invariant system in the dq0–frame using the instantaneous active and reactive power theory, which has similar control performance to the traditional VOC strategy when the phase angle is correctly detected. In addition, it has both DPC and traditional VOC advantages simultaneously with lower computational complexity. On the other hand, in GC-VSIs, a properly current controller is necessary to achieve the aforementioned performances.

Various techniques have been developed to achieve these performances. Even though a PI controller offers performance advantages such as simplicity, low iterative parameters, and easy implementation. Still, there are several challenges that these controllers cannot overcome, linked to the coupling effect and robustness toward parametric variations and external disturbances [14].

Nowadays, many studies have paid great attention to the sliding mode controller (SMC) in power converter control and have confirmed its ability to resolve all PI controller problems and limitations. The SMC based on Lyapunov functions is highly robust, stable, and less sensitive to many uncertainties and linearities than the PI controllers [14–16]. However, the chattering effect of the SMC is a major drawback in controlling the GC-VSI systems.

The Super Twisting SMC (STSMC) is considered an extension of the classical SMCs (CSMCs) and has been recognized as an effective control technique due to its advantages of high robustness, excellent static and dynamic performance, ease of designation and implementation, and the ability to resolve the chattering problem that exists in most CSMCs [15,16]. In addition, it is alleged that the effective implementation of STSMC results in highly asymptotic stability with finite-time convergence to zero, reliability, and accuracy, unlike the CSMC in the existence

[1] Electrical Engineering Laboratory (EEL), University of Msila, Algeria. E-mails: ali.chebabha@univ-msila.dz; aldawah.alaa@univ-msila.dz; mabrouk.defdaf@univ-msila.dz
[2] LPMRN Laboratory, University of Bordj Bou Arreridj, El-Anasser, Algeria. E-mail: abdelhalim.kessal@univ-bba.dz

of measurement errors and switching delays [16]. The control objective of STSMC is to lead both the sliding surface and its derivative to zero asymptotically in finite time, which is achieved through a discontinuous control action [15]. The concept of this technique is to choose an appropriate sliding surface and Lyapunov function depending on the control objectives of the overall system, which can achieve excellent steady-state performance while preserving the prominent features of the SMC, such as robustness, stability, and simplicity [16].

This work proposes an enhanced VOC strategy based on DPC concepts (EVOC) to eliminate the impact of PLL and Park's transformation and achieve accurate current control in the dq0–frame with lower computational complexity. For the GC-FLVSI current controllers, the STSMC technique is proposed to improve the static and dynamic performances and obtain high robustness against parametric variations with simple implementation. Transient and steady-state performances of the proposed EVOC-STSMC strategy for GC-FLVSI are evaluated and compared with those based on PIC regarding response, steady-state errors, zero-sequence current and THDs mitigation, neutral current reduction, and robustness against parameter variations. The proposed control strategy for GC-FLVSI illustrates satisfactory results for all the previous performance indicators, demonstrating the proposed strategy's superiority and effectiveness.

This paper is organized as follows: in section 2, the model of the FLVSI in the dq0-frame using the DPC concepts is presented. Then, detailed output current control loops using the proposed STSMC are developed and detailed in section 3. Section 4 presents the simulation results and discusses the viability and superiority of the proposed EVOC-STSMC for FLVSI. Finally, Section 5 summarizes the conclusion of this work.

2. GRID-CONNECTED FOUR-LEG PWM VSI DQ0 MODELING-BASED POWER THEORY

The adopted power circuit of three-phase four–wire GC-FLVSI is illustrated in Fig. 1.

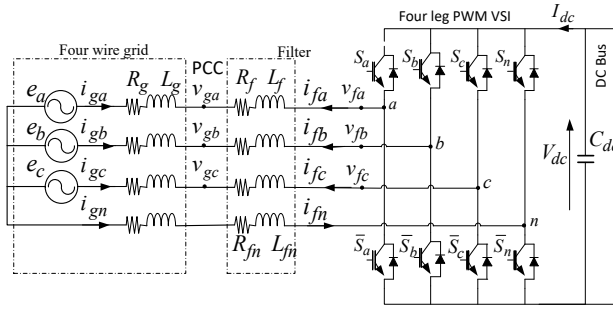

Fig. 1 – Power circuit of four wire grid connected FLVSI.

The output currents dynamic of GC-FLVSI shown in Fig. 1 can be defined in the abc-frame by [6] as:

$$\begin{cases} L_{fa}\frac{\mathrm{d}i_{fa}}{\mathrm{d}t} = -v_{ga} - R_{fa}i_{fa} + v_{fa} - R_{fn}i_n - L_{fn}\frac{\mathrm{d}i_n}{\mathrm{d}t} \\ L_{fb}\frac{\mathrm{d}i_{fb}}{\mathrm{d}t} = -v_{gb} - R_{fb}i_{fb} + v_{fb} - R_{fn}i_n - L_{fn}\frac{\mathrm{d}i_n}{\mathrm{d}t} \\ L_{fc}\frac{\mathrm{d}i_{fc}}{\mathrm{d}t} = -v_{gc} - R_{fc}i_{fc} + v_{fc} - R_{fn}i_n - L_{fn}\frac{\mathrm{d}i_n}{\mathrm{d}t} \end{cases}, \quad (1)$$

where v_{fabc} and i_{fabc} are the FLVSI output voltages and injected currents, respectively, v_{gabc} are the point of common coupling (PCC) voltages. i_{fn} is the neutral line current, and L_{fabcn} and R_{fabcn} are the filter inductors and their internal resistors, respectively.

Using Concordia transformation of the system (1), the dynamic model in the αβ0-frame is given as follows:

$$\begin{cases} \frac{\mathrm{d}i_{f\alpha}}{\mathrm{d}t} = -\frac{R_f}{L_f}i_{f\alpha} - \frac{v_{g\alpha}}{L_f} + \frac{v_{f\alpha}}{L_f} \\ \frac{\mathrm{d}i_{f\beta}}{\mathrm{d}t} = -\frac{R_f}{L_f}i_{f\beta} - \frac{v_{g\beta}}{L_f} + \frac{v_{f\beta}}{L_f} \\ \frac{\mathrm{d}i_{f0}}{\mathrm{d}t} = -\frac{R_f+3R_{fn}}{L_f+3L_{fn}}i_{f0} - \frac{v_{g0}-v_{f0}}{L_f+3L_{fn}} \end{cases}, \quad (2)$$

According to the instantaneous power theory [12], the grid active and reactive powers (p_g and q_g) can be calculated in the abc reference frame as follows:

$$\begin{cases} p_g = v_{ga}i_{fa} + v_{gb}i_{fb} + v_{gc}i_{fc} \\ q_g = \sqrt{1/3}\left[(v_{gb}-v_{gc})i_{fa} - (v_{gc}-v_{ga})i_{fb} + (v_{ga}-v_{gb})i_{fc}\right] \end{cases}, \quad (3)$$

These powers in the αβ0-frame are expressed as:

$$\begin{cases} p_g = v_{g\alpha}i_{f\alpha} + v_{g\beta}i_{f\beta} + v_{g0}i_{f0} \\ q_g = v_{g\beta}i_{f\alpha} - v_{g\alpha}i_{f\beta} \end{cases}, \quad (4)$$

By considering that the grid voltages are balanced (v_{g0}=0), the dynamics of these powers in (4) are given as:

$$\begin{cases} \frac{\mathrm{d}p_g}{\mathrm{d}t} = v_{g\alpha}\frac{\mathrm{d}i_{f\alpha}}{\mathrm{d}t} + i_{f\alpha}\frac{\mathrm{d}v_{g\alpha}}{\mathrm{d}t} + v_{g\beta}\frac{\mathrm{d}i_{f\beta}}{\mathrm{d}t} + i_{f\beta}\frac{\mathrm{d}v_{g\beta}}{\mathrm{d}t} \\ \frac{\mathrm{d}q_g}{\mathrm{d}t} = v_{g\beta}\frac{\mathrm{d}i_{f\alpha}}{\mathrm{d}t} + i_{f\alpha}\frac{\mathrm{d}v_{g\beta}}{\mathrm{d}t} - v_{g\alpha}\frac{\mathrm{d}i_{f\beta}}{\mathrm{d}t} - i_{f\beta}\frac{\mathrm{d}v_{g\alpha}}{\mathrm{d}t} \end{cases}, \quad (5)$$

These power dynamics consist mainly of the injected current and the grid voltage dynamics. To simplify these dynamics, we consider that the grid voltages are balanced. Thus, the grid voltages in the αβ0-frame can be obtained as:

$$\begin{cases} v_{g\alpha} = V_{gm}\cos(\omega t) \\ v_{g\beta} = V_{gm}\sin(\omega t) \\ v_{g0} = 0 \end{cases}, \quad (6)$$

where V_{gm} is the grid voltage magnitude, expressed as:

$$V_{gm} = \sqrt{v_{g\alpha}^2 + v_{g\beta}^2}, \quad (7)$$

The derivative of (6) gives:

$$\begin{cases} \frac{\mathrm{d}v_{g\alpha}}{\mathrm{d}t} = -\omega V_{gm}\sin(\omega t) \\ \frac{\mathrm{d}v_{g\beta}}{\mathrm{d}t} = \omega V_{gm}\cos(\omega t) \end{cases}, \quad (8)$$

Substituting (2), (4), and (8) into (5), we obtain:

$$\begin{cases} \frac{\mathrm{d}p_g}{\mathrm{d}t} = -\frac{R_f}{L_f}p_g - \omega q_g + \frac{1}{L_f}\left(v_{g\alpha}v_{f\alpha} + v_{g\beta}v_{f\beta} - V_{gm}^2\right) \\ \frac{\mathrm{d}q_g}{\mathrm{d}t} = \omega p_g - \frac{R_f}{L_f}q_g + \frac{1}{L_f}\left(v_{g\beta}v_{f\beta} - v_{g\alpha}v_{f\alpha}\right) \end{cases}, \quad (9)$$

It can be observed from (8) that the grid power dynamic model is a multi-input multi-output (MIMO) system, where the FLVSI output voltages $v_{f\alpha}$ and $v_{f\beta}$ are the original control inputs and the grid powers p_g and q_g are the outputs. We also observe that this dynamic is a time-variant (TV) system, where $v_{f\alpha}$ and $v_{f\beta}$ are multiplied simultaneously by $v_{g\alpha}$ and $v_{g\beta}$. To simplify this model, two new control inputs, $v_{p,}$ and v_q, are introduced as follows:

$$\begin{cases} v_p = v_{g\alpha}v_{f\alpha} + v_{g\beta}v_{f\beta} \\ v_q = v_{g\beta}v_{f\alpha} - v_{g\alpha}v_{f\beta} \end{cases}. \quad (10)$$

By using (6), the new control inputs v_p and v_q become:

$$\begin{bmatrix} v_p \\ v_q \end{bmatrix} = V_{gm} \begin{bmatrix} \cos(\omega t) & \sin(\omega t) \\ \sin(\omega t) & -\cos(\omega t) \end{bmatrix} \begin{bmatrix} v_{f\alpha} \\ v_{f\beta} \end{bmatrix} = V_{gm} \begin{bmatrix} v_{fd} \\ v_{fq} \end{bmatrix}, \quad (11)$$

where v_{fd} and v_{fq} are the FLVSI output voltages in the dq0-frame, obtained through the control inputs in (10) without using Park's transformation.

Using (10), the power dynamics in (9) become:

$$\begin{cases} \frac{\mathrm{d}p_g}{\mathrm{d}t} = -\frac{R_f}{L_f} p_g - \omega q_g + \frac{1}{L_f}\left(v_p - V_{gm}^2\right) \\ \frac{\mathrm{d}q_g}{\mathrm{d}t} = \omega p_g - \frac{R_f}{L_f} q_g + \frac{1}{L_f} v_q \end{cases}, \quad (12)$$

Note that the grid power dynamics in (12) are a MIMO and a time-invariant (TI) system with a coupling effect between active and reactive powers and have the same structure as the FLVSI injected current dynamic model in the dq0–frame [11]. Then, we will present the relationship between these models. When v_{gd} is oriented to the grid voltage vector, and v_{gq} is in quadrature with it, $v_{gd}=V_{gm}$ and $v_{gq}=0$ in the VOC strategy, the grid active and reactive powers can be calculated in the dq-frame as follows:

$$\begin{cases} p_g = V_{gm} i_{fd} \\ q_g = V_{gm} i_{fq} \end{cases}, \quad (13)$$

Substituting (11) and (13) into (12) and by the consideration of zero-sequence current i_{f0}, which does not need PT to be obtained, the new dq FLVSI injected current dynamic model can be derived from the grid power dynamic model as follows:

$$\begin{cases} \frac{\mathrm{d}i_{fd}}{\mathrm{d}t} = -\frac{R_f}{L_f} i_{fd} - \omega i_{fq} - \frac{V_{gm}}{L_f} + \frac{v_{fd}}{L_f} \\ \frac{\mathrm{d}i_{fq}}{\mathrm{d}t} = -\frac{R_f}{L_f} i_{fq} + \omega i_{fd} + \frac{v_{fd}}{L_f} \\ \frac{\mathrm{d}i_{f0}}{\mathrm{d}t} = -\frac{R_f + 3R_{fn}}{L_f + 3L_{fn}} i_{f0} - \frac{v_{g0} - v_{f0}}{L_f + 3L_{fn}} \end{cases}, \quad (14)$$

i_{fdq0} and v_{fdq0} are the dq0 FLVSI injected currents and output voltages, respectively, and ω is the grid angular frequency. The zero-sequence current i_{f0} is given by:

$$i_{f0} = \sqrt{1/3}\left(i_{fa} + i_{fb} + i_{fc}\right) = \sqrt{1/3}\, i_n, \quad (15)$$

Note that the new grid power dynamic model in (12) is changed into the traditional dq0 FLVSI injected current model (14) without PLL and Park transformation.

3. PROPOSED EVOC-STSMC STRATEGY OF GRID-CONNECTED FOUR-LEG INVERTER

The proposed control scheme in the dq0–frame for the GC-FLVSI is shown in Fig. 2. As it is shown in this figure, the STSMC and the dq0 determine the FLVSI output voltage references–axes injected currents are provided through DPC theory without using Park's transformation. The three-dimensional space vector modulation (3DSVPWM) technique described in [18] is considered in this work due to its constant switching frequency and low injected current THDs.

The STSMC objective of the FLVSI injected currents is to lead their tracking error sliding surfaces with their derivatives to zero in finite time, carried through discontinuous control actions based on the ST algorithm. According to (14), there are coupling terms between dq-axes injected currents i_{fd} and i_{fq}.

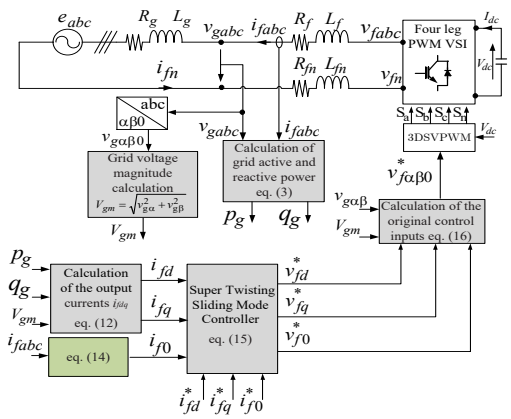

Fig. 2 – Proposed EVOC-STSMC circuit schematic of the GC-FLVSI.

These couplings are mitigated using the proposed STSMC-based VOC strategy by the introductions of ST actions to the equivalent SMC laws in the dq0 output voltage references as follows:

$$\begin{cases} v_{fd}^* = v_{fd\text{-}eq}^* + v_{fd\text{-}ST}^* \\ v_{f0}^* = v_{fq\text{-}eq}^* + v_{fq\text{-}ST}^* \\ v_{f0}^* = v_{f0\text{-}eq}^* + v_{f0\text{-}ST}^* \end{cases}, \quad (16)$$

where $v_{fdq0\text{-}eq}^*$ and $v_{fdq0\text{-}ST}^*$ are the equivalent SMC laws and the ST discontinuous control actions, respectively.

Using the control inputs v_{fdq0}^* in (16) and the inverse of (11), the original control inputs $v_{f\alpha\beta0}^*$ required by the 3DSVPWM technique, are obtained without using Park's transformation, as illustrated in Fig. 2, as follows:

$$\begin{bmatrix} v_{f\alpha}^* \\ v_{f\beta}^* \\ v_{f0}^* \end{bmatrix} = \frac{1}{V_{gm}} \begin{bmatrix} v_{g\alpha} & v_{g\beta} & 0 \\ v_{g\beta} & -v_{g\alpha} & 0 \\ 0 & 0 & 1 \end{bmatrix} \begin{bmatrix} v_{fd}^* \\ v_{fq}^* \\ v_{f0}^* \end{bmatrix}, \quad (17)$$

The tracking error sliding surfaces for the dq0 FLVSI injected currents are given as follows [15]:

$$\begin{cases} S_d = i_{fd} - i_{fd}^* \\ S_q = i_{fq} - i_{fq}^* \\ S_0 = i_{f0} - i_{f0}^* \end{cases}, \quad (18)$$

where S_d, S_d, and S_0 are the dq0–axes tracking error sliding surfaces, respectively.

Using the dq0 FLVSI model in (13), the derivatives of the three sliding surfaces can be written as:

$$\begin{cases} \dot{S}_d = -\frac{R_f}{L_f} i_{fd} - \omega i_{fq} - \frac{V_{gm}}{L_f} + \frac{v_{fd}}{L_f} - i_{fd}^* \\ \dot{S}_q = -\frac{R_f}{L_f} i_{fq} + \omega i_{fd} + \frac{v_{fd}}{L_f} - i_{fq}^* \\ \dot{S}_0 = -\frac{R_f + 3R_{fn}}{L_f + 3L_{fn}} i_{f0} - \frac{v_{g0} - v_{f0}}{L_f + 3L_{fn}} - i_{f0}^* \end{cases}, \quad (19)$$

Setting $\dot{S}_{dq0}=0$, then the equivalent control laws $v_{fdq0\text{-}eq}^*$ of the dq0 injected currents can be obtained as:

$$\begin{cases} v_{fd\text{-}eq}^* = L_f\left(\frac{R_f}{L_f} i_{fd} + \omega i_{fq} + \frac{V_{gm}}{L_f} + i_{fd}^*\right) \\ v_{fq\text{-}eq}^* = L_f\left(\frac{R_f}{L_f} i_{fq} - \omega i_{fd} + i_{fq}^*\right) \\ v_{f0\text{-}eq}^* = \left(L_f + 3L_{fn}\right)\left(\frac{R_f + 3R_{fn}}{L_f + 3L_{fn}} i_{f0} + i_{f0}^*\right) \end{cases}, \quad (20)$$

The discontinuous control actions $v^*_{fdq0\text{-}ST}$ are designed based on the ST algorithm as follows [15]:

$$\begin{cases} v^*_{fd\text{-}ST}=-\rho_d|S_d|^{\frac{1}{2}}sing(S_d)-\lambda_d\int sing(S_d)dt \\ v^*_{fq\text{-}ST}=-\rho_q|S_q|^{\frac{1}{2}}sing(S_q)-\lambda_q\int sing(S_q)dt \\ v^*_{f0\text{-}ST}=-\rho_0|S_0|^{\frac{1}{2}}sing(S_0)-\lambda_0\int sing(S_0)dt \end{cases}, \quad (21)$$

where ρ_{dq0} and λ_{dq0} are positive constants, which are chosen to achieve good control performance while considering the demands of stability, robustness, and dynamic response as follows [16]: $\rho_{dq0}=15\times10^6$ and $\lambda_{dq0}=4\times10^5$.

On the other hand, the output control variables of the PICs used in the current inner loops are given as follows:

$$v^*_{fdq0}=\left(i_{fdq0}-i^*_{fdq0}\right)\left(k_p+\frac{k_i}{s}\right), \quad (22)$$

k_p and k_i are the gains of the PICs, which are calculated using the pole placement method as follows [6]:

$$\begin{cases} k_{p\text{-}dq}=2L_f\zeta\omega_n-R_f \\ k_{i\text{-}dq}=L_f\omega_n^2 \\ k_{p\text{-}0}=2\left(L_f+3L_{fn}\right)\zeta\omega_n-\left(R_f+3R_{fn}\right) \\ k_{i\text{-}0}=\left(L_f+3L_{fn}\right)\omega_n^2 \end{cases}, \quad (23)$$

where ω_n and ξ are PIC's natural frequency and damping factor, respectively. ξ is set to 0.707 for suitable overshoot under a transient process, and ω_n is set to 3×10^3 rad/s for the adjustment between dynamic responses and immunity versus distortion and harmonic currents.

4. SIMULATION STUDY

To confirm the viability and effectiveness of the proposed EVOC-STSMC, simulation scenario tests have been developed on MATLAB/Simulink using Sim Power Systems and S-Function based on C. The system and simulation parameters are presented in Table 1.

Table 1

System simulation parameters

Parameter	Value
Grid voltage (RMS) Vg	110 V
Grid frequency	50 Hz
DC-bus voltage Vdc	350V
Filter inductance and resistance L_f and R_f	5 mH, 0.15 Ω
neutral filter inductance L_{fn}	2 mH
Switching frequency fs	15 kHz

The main indicators considered to check the behavior of the GC-FLVSI are the FLVSI currents i_{fabcn} with their THDs, their dq0–axes components i_{fdq0}, and essentially the grid active and reactive powers. The control errors of current i_{fdq0} are also represented and analyzed in terms of criteria, including integral-time-absolute-error (ITAE) and integral-time-square-error (ITSE). These error performance indexes of the control output x (i_{fd}, i_{fq} and i_{f0}) and its reference x^* are defined as:

$$\begin{cases} ITAE=\int_0^t t|x\text{-}x^*|dt \\ ITSE=\int_0^t t\left(x\text{-}x^*\right)^2dt \end{cases}, \quad (24)$$

At first, a comparative study between both controllers (PIC and STSMC) based proposed EVOC strategy during ideal grid voltage when i_{fd} change from 5 to 10 A at 0.02 s and i_{fq} change from 0 to -5 A at 0.06 s is achieved, as shown in Fig. 3. The oscillation magnitude values for each current (i_{fd}, i_{fq}, i_{f0} and i_n) and the integral error performance index (ITAE and ITSE) values for each controller are analyzed and illustrated in Tables 2 and 3, respectively. Also, Figs. 4 (a, b, and c) compare the transient and steady-state responses of dq0 currents before and after i_{fdq} changes.

According to these figures, the dq-axes injected currents have current oscillations before and after these changes and overshoot at the changes. In this, the dq0 inject currents reach their references with fast responses at the starting of FLVSI and at the changes of i_{fd} and i_{fq} with small oscillations and overshoots before and after these changes using proposed EVOC-STSMC compared to the EVOC-PIC as shown in Figs. 3 (a and b). The zero-sequence current i_{f0} is kept constant at zero before and after these changes with small oscillations also using proposed EVOC-STSMC Fig. 3 (c). Moreover, the performance of active and reactive powers with proposed EVOC-STSMC is very good as well as shown in Fig. 3 (d).

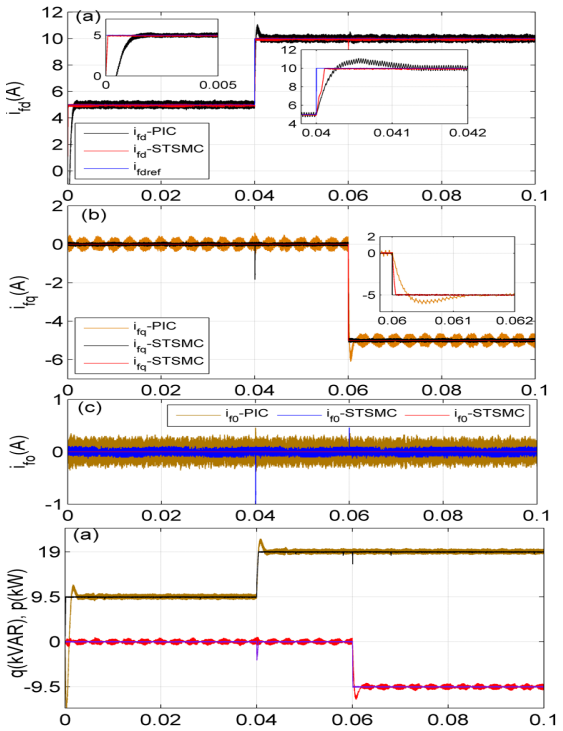

Fig. 3 – Comparative study between both strategy in transient and steady states when i_{fd} and i_{fq} changes under ideal grid voltage: (a) d-axis inject current; (b) q-axis inject current; (c) zero-sequence current i_{f0}; (d) grid active and reactive powers.

The three-phase injected and neutral currents (i_{gabcn}) using both controllers are illustrated in Fig. 4 (a and b). It can be observed from these figures that the injected currents are sinusoidal before and after the changes of i_{fd} and i_{fq} with very small ripples and THDs using the proposed EVOC-STSMC compared to the EVOC-PIC. It can also clearly be observed from these figures that the maximum neutral grid current oscillation is also ideally reduced from 0.72 A using EVOC-PIC to 0.25 A using proposed EVOC-STSMC before and after these changes, as also shown in Table 2. Using EVOC-PIC, the THD values are 2.22 %, significantly reduced to 1.25% using the proposed EVOC-STSMC in Fig. 5, which fits the IEEE 519 standard. In addition, the error performance indexes illustrated in Table 2 and the oscillation magnitude values of each current listed in Table 3 demonstrate that the values of these criteria have been enhanced by using the proposed EVOC-STSMC.

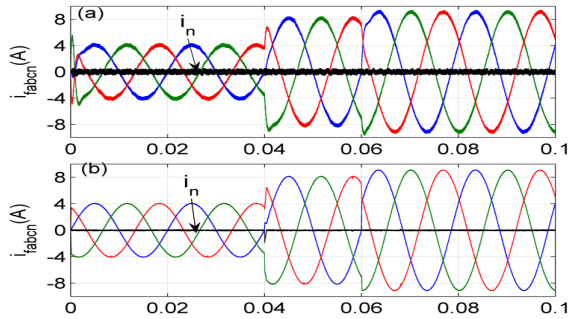

Fig. 4 – Three-phase inject and neutral currents (i_{gabcn}) under ideal grid voltage: (a) EVOC-PIC; (b) proposed EVOC-STSMC

Figure 5 compares the injected current THDs versus filter inductance using both controllers when the filter inductance varies from 2.5 to 7.5 mH. This comparative study shows that the THDs decreased from 2.45 to 0.45 % using the STSMC and from 3.98 to 1.57 % using the PIC, which demonstrates again the superiority and robustness of the proposed STSMC.

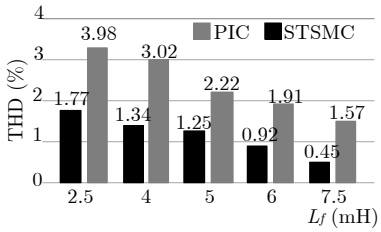

Fig. 5 – Injected current THD versus filter inductor variation

To evaluate the performance of the proposed EVOC strategy based on both control techniques under unbalanced grid voltages, a 20 % voltage sag in the first phase is performed as illustrated in Fig. 6.

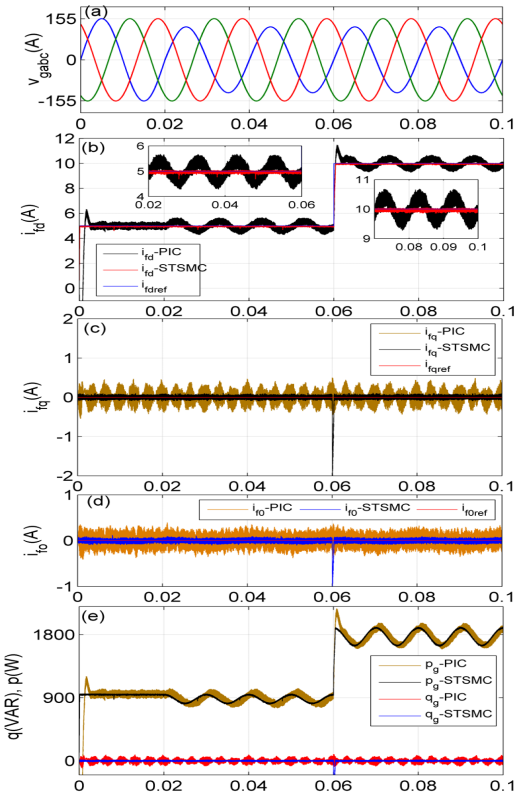

Fig. 6 – Comparative study between both strategy in transient and steady states when i_{fd} change under a 20% voltage sag in the phase a: (a) unbalanced grid voltages; (b) d-axis inject current; (c) q-axis inject current; (d) zero-sequence current i_{f0}; (e) active and reactive powers.

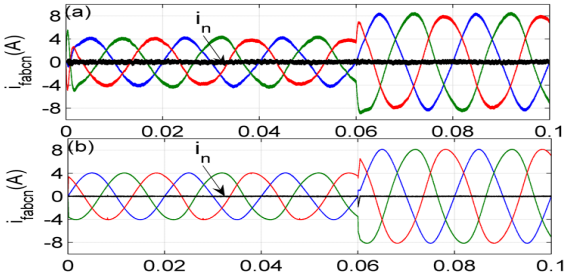

Fig. 7 – Three-phase inject and neutral currents (i_{gabcn}) under a 20% voltage sag in the phase a: (a) EVOC-PIC; (b) proposed EVOC-STSMC

As shown in Fig. 6 (b), the first phase voltage sag cause second-order harmonic ripples in the d-axis injected current when the EVOC-PIC is used. These ripples cause high distortion on the three-phase injected currents (Fig. 7(a)) with a large magnitude of the 3rd harmonic, as shown in the FFT analysis illustrated in Fig. 8 (a). With the proposed EVOC-STSMC, the d-axis injected current is not affected by the grid voltage sag, and the second-order harmonic ripples are almost totally suppressed with a very fast response Fig. 6 (b); the 3rd harmonic in the injected currents is further reduced to very small values compared with EVOC-PIC (Fig. 8 (b)), which demonstrate the straight dominance of the proposed EVOC-STSMC under grid voltage sag. The q0-axes injected currents track their references under voltage sag with very smaller oscillations using the proposed EVOC-STSMC, as shown in Figs. 8 (c and d). The behavior of the neutral current is almost the same before and after voltage sag with very small oscillations using the proposed EVOC-STSMC as shown in Figs. 7 (a and b).

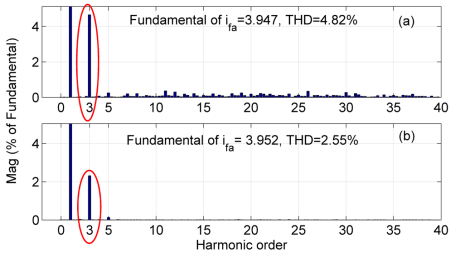

Fig. 8 – FFT of the first phase FLVSI injected current: (a) EVOC-PIC; (b) proposed EVOC-STSMC

When comparing this case to the ideal grid voltage case, the THD values in the EVOC-PIC increases from 2.22 % for the three phases to 4.82 %, 4.60 %, and 4.64 % in phases a, b, and c, respectively, where, using the proposed EVOC-STSMC, these THD values increased from 1.25 % for three phases to 2.55 %, 2.46 % and 2.48 % in phases a, b, and c, respectively, in this, the proposed EVOC-STSMC is superior compared to the EVOC-PIC.

Table 2

Oscillations in FLVSI injected current

Output current	Oscillations (A)	
	PIC	STSMC
i_{fd}	0.8A	0.2A
i_{fq}	1A	0.24A
i_{f0}	0.8A	0.2A

Table 3

Error performance indexes

	PIC			STSMC		
	i_{fd}	i_{fq}	i_{f0}	i_{fd}	i_{fq}	i_{f0}
ITAE	$2.13.10^{-3}$	$4.86.10^{-2}$	$2.39.10^{-2}$	$1.05.10^{-4}$	$1.22.10^{-3}$	$1.46.10^{-3}$
ITSE	$3.04.10^{-3}$	$4.22.10^{-3}$	$4.34.10^{-3}$	$1.18.10^{-4}$	$0.07.10^{-3}$	$1.89.10^{-4}$

5. CONCLUSION

An enhanced vector-oriented control (EVOC) strategy in the dq0–frame without using PLL based on super twisting sliding mode control (STSMC) for an FLVSI has been presented. The control performance regarding response, tracking references, overshoots, oscillation, and steady-state errors is achieved under both ideal and non-ideal grid voltage. This strategy is used for GC-FLVSI synchronization and control and to provide the GC-FLVSI module in the dq0–frame. This proposed EVOC-STSMC strategy is validated in various scenarios using MATLAB/Simulink. Moreover, the proposed EVOC-STSMC has been compared to EVOC-PIC. In contrast to the EVOC-PIC, the proposed EVOC-STSMC can achieve high performance and dynamic responses under ideal and non-ideal grid voltage without needing a PLL but will have a high quality of injected currents where the grid voltage is unbalanced. We can anticipate, in summary, the following features of the proposed EVOC-STSMC strategy:

1. The proposed EVOC strategy does not need Park's transformation to provide a linear time-invariant grid-connected VSI in the dq0–frame. It can be provided easily by using the instantaneous power theory (DPC).
2. The proposed EVOC-STSMC strategy can stabilize the disturbance GC-VSI with a good performance.
3. Finally, the responses of the GC-FLVSI using the proposed EVOC-STSMC have much better quality than the EVOC-PI strategy under grid voltage disturbance.

Received on 18 May 2022

REFERENCES

1. J.G. Carrasco, C.A. Silva, R. Peña, R. Cárdenas, *Control of a four-leg converter for the operation of a DFIG feeding stand-alone unbalanced loads*, IEEE Tran. on Ind. Electr, **62**, *7*, pp. 4630–4640 (2014).
2. M. R. Miveh, M. F. Rahmat, A. A. Ghadimi, M. W. Mustafa, *Control techniques for three-phase four-leg voltage source inverters in autonomous microgrids: A review*, Renewable and Sustainable Energy Reviews, **54**, pp. 1592–1610 (2016).
3. R. Mandrioli, A. Viatkin, M. Hammami, M. Ricco, G. Grandi, *A comprehensive ac current ripple analysis and performance enhancement via discontinuous PWM in three-phase four-leg grid-connected inverters*, Energies, **13**, *17*, pp. 4352 (2020).
4. A. Chebabhi, M.K. Fellah, M.F. Benkhoris, A. Kessal, *Artificial neural network based synchronous reference frame theory in the dq0 axes for reference harmonic currents generation of a four leg shunt active power filter,* Rev. Roum. Sci. Techn. – Électrotechn. Et Énerg., **61**, *4*, pp. 408–4013 (2016).
5. J.C. Olives-Camps, J.M. Mauricio, M. Barragán-Villarejo, F.J. Matas-Díaz, *Voltage control of four-leg VSC for power system applications with nonlinear and unbalanced loads*, IEEE Trans. on Energy Conversion., **35**, *2*, pp. 640–650 (2019).
6. A. Djerioui, A. Houari, A. Saim, M. Aït-Ahmed, S. Pierfederici, M.F. Benkhoris, M. Ghanes, *Flatness-based grey wolf control for load voltage unbalance mitigation in four-leg voltage source inverters*, IEEE Trans. on Ind. Appl., **56**, *2*, pp. 1869–1881 (2019).
7. Y., Song, F. Blaabjerg, *Analysis of middle-frequency resonance in DFIG system considering phase-locked loop*, IEEE Trans. on Power Electr., **33**, *1*, pp. 343–356 (2017).
8. Z. Ali, N. Christofides, E. Kyriakides, Y. Yang, F. Blaabjerg, *Three-phase phase-locked loop synchronization algorithms for grid-connected renewable energy systems: A review*, Renewable and Sustainable Energy Reviews, **90**, pp. 434–452 (2018).
9. R. Bimarta, K.H. Kim, *A robust frequency-adaptive current control of a grid-connected inverter based on LMI-LQR under polytopic uncertainties*, IEEE Power Energy Society Section, **8**, pp. 28756–28773 (2020).
10. X. Zheng, L. Xiao, Z. Wang, Y. Lei, C. Wang, *Control strategy without phase-locked loop based on coordinate transformation for three-phase AC/DC converter*. IET Power Electronics, **8**, *9*, pp. 1701–1709 (2015).
11. Y. Gui, X. Wang, F. Blaabjerg, *Vector current control derived from direct power control for grid-connected inverters*, IEEE Transactions on Power Electronics, **34**, *9*, pp. 9224–9235 (2018).
12. P. Cheng, C. Wu, F. Ning, J. He, *Voltage modulated DPC strategy of DFIG using extended power theory under unbalanced grid voltage conditions*, Energies, **13**, *22*, pp. 6077 (2020).
13. M. Alqatamin, J. Latham, Z.T. Smith, B.M. Grainger, M.L. McIntyre, *current control of a three-phase, grid-connected inverter in the presence of unknown grid parameters without a phase-locked loop*, IEEE Journal of Emerging and Selected Topics in Power Electronics, **9**, *3*, pp. 3127–3136 (2020).
14. K.R.S.Vadivu, R. Ramaprabha, *Improved steady state and large signal transient response of three-level ac-dc converter using hysteresis modulation based SMC under DCM*, Rev. Roum. Sci. Techn. – Électrotechn. Et Énerg., 66, *2*, pp. 85–90 (2021).
15. S. Biricik, H. Komurcugil, H. Ahmed, *Super twisting sliding-mode control of DVR with frequency-adaptive Brockett oscillator*. IEEE Trans. on Ind. Electr., **68**,*11*, 10730–10739 (2020).
16. B. Kelkoul, A. Boumediene, *Stability analysis and study between classical sliding mode control (SMC) and super twisting algorithm (STA) for doubly fed induction generator (DFIG) under wind turbine*, Energy, **214**, pp. 118871 (2021).
17. S. Ozdemir, N. Altin, I. Sefa, Z. Zhang, H. Komurcugil, *Super twisting sliding mode control of three-phase grid-tied neutral point clamped inverters*. ISA transactions, **125**, pp. 547–559 (2022).
18. A. Chebabhi, M.K. Fellah, M.F. Benkhoris, *3D space vector modulation control of four-leg shunt active power filter using pq0 theory*, Rev. Roum. Sci. Techn. – Électrotechn. Et Énerg., **60**, *2*, pp. 371–376 (2015).